

CHE-9023294 from the National Science Foundation and a Fulbright Fellowship to R.H.S.

References and Notes

- (1) Part 78 in the series: Systematic Design of Chemical Oscillators. Part 77: Rábai, G.; Orbán, M.; Epstein, I. R. *J. Phys. Chem.* **1992**, *96*, 5414.
- (2) De Kepper, P.; Epstein, I. R.; Kustin, K. *J. Am. Chem. Soc.* **1981**, *103*, 2133.
- (3) Orbán, M.; Dateo, C.; De Kepper, P.; Epstein, I. R. *J. Am. Chem. Soc.* **1982**, *104*, 5911.
- (4) Alamgir, M.; Epstein, I. R. *J. Phys. Chem.* **1985**, *89*, 3611.
- (5) Dateo, C.; Orbán, M.; De Kepper, P.; Epstein, I. R. *J. Am. Chem. Soc.* **1982**, *104*, 504.
- (6) Khan, A. B.; Higginson, W. C. E. *J. Chem. Soc., Dalton Trans.* **1981**, 2537.
- (7) Orbán, M.; De Kepper, P.; Epstein, I. R. *J. Phys. Chem.* **1982**, *86*, 431.
- (8) Nagypál, I.; Epstein, I. R. *J. Phys. Chem.* **1986**, *90*, 6285.
- (9) Orbán, M.; Epstein, I. R. *J. Phys. Chem.* **1982**, *86*, 3907.
- (10) Simoyi, R. H.; Masere, J.; Mutimbaranda, C.; Manyonda, M.; Dube, S. *Int. J. Chem. Kinet.* **1991**, *23*, 419.
- (11) Nagypál, I.; Bazsa, G.; Epstein, I. R. *J. Am. Chem. Soc.* **1986**, *108*, 3635.
- (12) Simoyi, R. H.; Manyonda, M.; Masere, J.; Mtambo, M.; Ncube, I.;

- Patel, H.; Epstein, I. R.; Kustin, K. *J. Phys. Chem.* **1991**, *95*, 770.
- (13) Capozzi, G.; Modena, G. *The Chemistry of the Thiol Group, Part 2*; Wiley & Sons: New York, 1974; pp 785-839.
- (14) Simoyi, R. H.; Noyes, R. M. *J. Phys. Chem.* **1987**, *91*, 2689.
- (15) Alamgir, M.; Epstein, I. R. *Int. J. Chem. Kinet.* **1985**, *17*, 429.
- (16) Simoyi, R. H. *J. Phys. Chem.* **1985**, *89*, 3570.
- (17) Lengyel, I.; Rábai, Gy.; Epstein, I. R. *J. Am. Chem. Soc.* **1990**, *112*, 904.
- (18) Davies, C. W. *J. Chem. Soc.* **1938**, 2093.
- (19) Bishop, E., Ed. *Indicators*; Pergamon Press: New York, 1972; p 195.
- (20) Feil, D.; Loong, W. S. *Acta Crystallogr., Sect. B* **1968**, *B24*, 1334.11.
- (21) Eigen, M.; Kustin, K. *J. Am. Chem. Soc.* **1962**, *84*, 1355.
- (22) Peintler, G.; Nagypál, I.; Epstein, I. R. *J. Phys. Chem.* **1990**, *94*, 2954.
- (23) Kieffer, R. G.; Gordon, G. *Inorg. Chem.* **1968**, *7*, 239.
- (24) Rábai, Gy.; Beck, M. T. *J. Chem. Soc., Dalton Trans.* **1985**, 1669.
- (25) Kaps, P.; Rentrop, P. *Numer. Math.* **1979**, *23*, 55.
- (26) Szivoczka, L.; Nagypál, I.; Boga, E. *J. Am. Chem. Soc.* **1989**, *111*, 2842.
- (27) Resch, P.; Field, R. J.; Schneider, F. W.; Burger, M. *J. Phys. Chem.* **1989**, *93*, 8186.
- (28) Rábai, Gy.; Orbán, M.; Epstein, I. R. *J. Phys. Chem.* **1992**, *96*, 5414.
- (29) Zhang, Y.-X.; Field, R. J. *J. Phys. Chem.*, submitted for publication.
- (30) Simoyi, R. H.; Epstein, I. R.; Kustin, K. *J. Phys. Chem.*, in press.
- (31) Simoyi, R. H.; Epstein, I. R.; Kustin, K. Manuscript in preparation.

Relaxation Kinetics and Infrared Spectra of the Complexation of Lithium Ion by Triethylene Glycol and by Tetraethylene Glycol in Acetonitrile

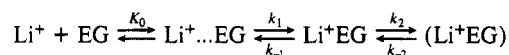
Daryl P. Cobranchi, Ben A. Garland, Marilyn C. Masiker, Edward M. Eyring,*

Department of Chemistry, University of Utah, Salt Lake City, Utah 84112

Paul Firman, and Sergio Petrucci

Weber Research Institute, Polytechnic University, Long Island Center, Route 110, Farmingdale, New York 11735 (Received: January 6, 1992; In Final Form: March 31, 1992)

Ultrasonic absorption relaxation spectra are reported covering the frequency range ~ 1 –500 MHz for the complexation of LiClO_4 by the open-chain polyethers triethylene glycol (EG3) and tetraethylene glycol (EG4) in acetonitrile at 25 °C and at a molar ratio $R = [\text{EG3}]/[\text{LiClO}_4]$ or $R = [\text{EG4}]/[\text{LiClO}_4] = 1$. The ultrasonic spectra can be described by the sum of two Debye relaxation processes which were interpreted according to the Eigen-Winkler mechanism



(where EG denotes either EG3 or EG4), giving the rate constants k_1 , k_{-1} , k_2 , and k_{-2} . The first step is taken to be a preequilibrium step for which K_0 is calculated from classical statistical theory. The rate constants are compared with those of the corresponding process involving triglyme and poly(ethylene oxide) (PEO) previously reported. Infrared data for the 3800–3200- cm^{-1} region show a shift of 70 cm^{-1} to lower energy, indicating a strong interaction between the ethanolic oxygen of EG3 and the Li^+ ion.

Introduction

The kinetics and mechanism of Li^+ complexation are of interest in part because of biochemical¹ and electrochemical ramifications.² In a recent study of complexation of Li^+ by poly(ethylene oxide) (PEO) of average molar mass $\bar{M} \sim 15000$ and by triglyme (TG3) with $M = 178$ amu, Eschmann et al.³ observed two concentration-dependent relaxation processes which, at the molar ratio $R = [-\text{O}(\text{CH}_2)_2-]/[\text{LiClO}_4] = 4$, were independent of molecular chain length. Since PEO has terminal hydroxyl groups for each chain, whereas TG3 is "capped" by methoxy ($-\text{OCH}_3$) terminal groups, it is interesting to see whether by shortening the chain length of PEO down to a size comparable to that of TG3, a large difference in the complexation behavior of Li^+ with the polyether is observed.

Thus we here extend the study of Li^+ complexation to ligands such as triethylene glycol (EG3) and tetraethylene glycol (EG4). They differ from TG3 by the replacement of the terminal methyl groups by hydrogen atoms for both ligands as well as by the addition of one $-\text{CH}_2\text{CH}_2\text{O}-$ group in the case of EG4; see Figure 1. The interaction of the hydroxyl group with Li^+ has been

documented by infrared (IR) spectra in the 3800–3200- cm^{-1} region as reported below. Acetonitrile was used as the solvent for all the systems investigated as in the previous work with TG3 and PEO.³

Experimental Section

Two different cylindrical resonators were used by our two research groups independently in the frequency range 1–7 MHz,⁴ yielding identical results within experimental error ($\pm 1\%$).

For the 15–215-MHz frequency range a previously described⁵ laser Debye-Sears instrument was used. The 30–600-MHz frequency range was also studied with a pulse ultrasonic absorption apparatus.⁶ These two methods also yielded comparable results within experimental error.

A 983G computer assisted Perkin-Elmer infrared spectrometer was used to collect the digitized infrared spectra. The Perkin-Elmer sealed demountable cells equipped with NaCl windows were calibrated before each run by the fringe method. The instrument was set in the single-scan, slow-speed mode (filter no. 4), with no smoothing, to avoid distortion of the spectral envelope. The

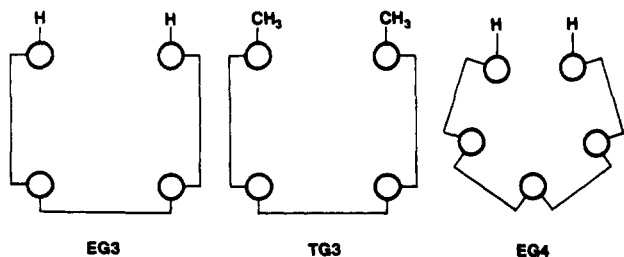


Figure 1. Formulas of triethylene glycol (EG3), triglyme (TG3), and tetraethylene glycol (EG4).

assisting computer records the digitized spectra in transmittance and converts them to digitized absorbances.

Anhydrous LiClO_4 (Aesar or Aldrich) was dried at $\sim 100^\circ\text{C}$ in vacuo for several days until constancy of weight was obtained. LiAsF_6 and LiSO_3CF_3 were also dried in vacuo at 70°C .

Triethylene glycol (Aldrich) and tetraethylene glycol (Aldrich) were dried over activated 4A molecular sieves and then vacuum distilled. Acetonitrile (either E. M. Science Spectroscopic grade or Aldrich Gold Label) was refluxed for a day over P_4O_{10} and then distilled. All solutions were prepared and used with minimal contact (<20 s) with the atmosphere.

Results

Infrared data show a dramatic shift in the $-\text{OH}$ stretching region ($\sim 3500\text{ cm}^{-1}$) when LiClO_4 is added to a solution of EG3 or of EG4 in CH_3CN , thus indicating an interaction between the oxygen of the $-\text{OH}$ group and Li^+ . Figure 2 presents plots of the digitized IR spectra showing this shift.

Unfortunately, the spectra in the relevant $800\text{--}950\text{ cm}^{-1}$ region related to the coil breathing of the polyether⁷ appear for the ethylene glycols to be too complicated for an unambiguous analysis by Gaussian-Lorentzian functions and assignment of the absorbance bands. Nevertheless, this region does show an interaction between Li^+ and the ethereal oxygens.

Figure 3 (parts A and B) shows representative plots of the excess sound absorption data per wavelength $\alpha_{\text{exc}}\lambda = \mu = (\alpha - Bf^2)u/f$ vs the frequency f . α is the total absorption coefficient, and Bf^2 is the absorption coefficient at a frequency f far above the relaxation frequencies f_1 and f_{II} . $B = (\alpha/f^2)_{f \gg f_1, f_{II}}$ is the corresponding background ratio, $\lambda = u/f$ is the acoustical wavelength, and u is the sound velocity. The data are interpreted by the sum of two Debye⁸ relaxation processes:

$$\mu = 2\mu_1 \frac{f/f_1}{1 + (f/f_1)^2} + 2\mu_{II} \frac{f/f_{II}}{1 + (f/f_{II})^2} \quad (1)$$

where μ_1 and μ_{II} are the maximum amplitudes of the excess sound absorption per wavelength at the relaxation frequencies f_1 and f_{II} respectively.

The fit between the experimental data and the calculated μ values expressed by the solid line in Figure 3 was obtained by a computer graphic method allowing for iterative changes of the parameters f_1 , μ_1 , f_{II} , μ_{II} , and B to achieve an optimum fit by both minimizing $|\mu - \mu_{\text{calc}}|$ and averaging the frequency dispersion of $|\mu - \mu_{\text{calc}}|$. Figure 3 (parts C and D) shows, in fact, the deviational plots of $[(\alpha/f^2) - (\alpha/f^2)_{\text{calc}}]\%$ vs the frequency f . The systematic deviations between 1 and 2 MHz in Figure 3C,D are due to increasing failure of the resonator cells at the lowest used frequencies (lack of linearity between the $(\Delta f)_{1/2}$, namely, the bandwidth at half-power of the Lorentzian resonant bands, and frequency). Table I reports the parameters used for all the concentrations investigated for $\text{LiClO}_4 + \text{EG3}$ and for $\text{LiClO}_4 + \text{EG4}$ in acetonitrile at 25°C and molar ratio $R = [\text{EG3}]/[\text{LiClO}_4] = 1$ or $[\text{EG4}]/[\text{LiClO}_4] = 1$.

Calculations and Discussion

Ultrasonic Data. Relaxation kinetics theory applied to the following Eigen-Winkler⁹ scheme:

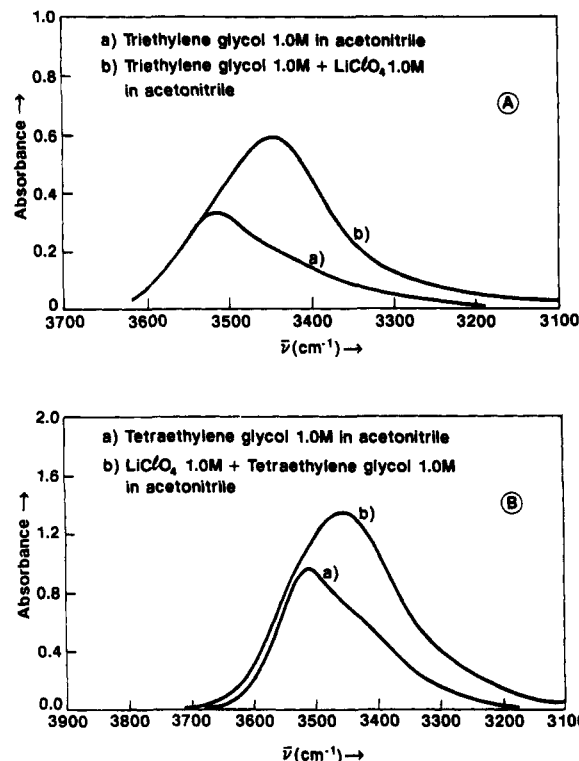
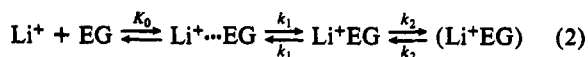


Figure 2. (A) Infrared spectrum of the $-\text{OH}$ stretch region for 1.0 M EG3 in acetonitrile and for 1.0 M EG3 + 1.0 M LiClO_4 in acetonitrile. (B) IR spectrum ($-\text{OH}$ stretch) for 1.0 M EG4 and for 1.0 M EG4 + 1.0 M LiClO_4 in acetonitrile.

leads to two observable relaxation times τ_1 and τ_{II} under the assumption of two closely coupled reaction steps (characterized by the rate constants k_1, k_{-1}, k_2, k_{-2}), both loosely coupled to a much faster preequilibration process (characterized by a preequilibration formation constant K_0).

In the above scheme, Li^+ and EG are the free lithium ion and either the EG3 or EG4 ligand in solution. $\text{Li}^+\cdots\text{EG}$ is a solvent separated species, Li^+EG is a contact species, and (Li^+EG) is a species with Li^+ embedded in the ethereal coil of the ethylene glycol ligand. Solution of the rate laws leads to the correlation between the sum S and the product P of the two relaxation times vs the rate constants and K_0 (Appendix I, eq 5A):

$$S = \tau_1^{-1} + \tau_{II}^{-1} = k_1 K_0 \frac{\theta}{1 + K_0 \theta} + k_{-1} + k_2 + k_{-2}$$

$$P + \tau_1^{-1} \tau_{II}^{-1} = k_1 K_0 \frac{\theta}{1 + K_0 \theta} (k_2 + k_{-2}) + k_{-1} k_{-2} \quad (3)$$

In the above, $\theta \simeq 2\alpha C$ where the degree of dissociation α is related to the overall complexation constant K_2 by the usual relation $K_2 = (1 - \alpha)/\alpha^2 C$, neglecting the activity coefficient ratios. The values of $K_2 = 50$ and $K_2 = 150$ for $\text{Li}^+ + \text{EG3}$ and $\text{Li}^+ + \text{EG4}$ respectively were taken from a ^7Li NMR investigation.¹⁰ $K_0 = [\text{Li}^+\cdots\text{EG}]/[\text{Li}^+][\text{EG}]$ has been calculated from the Fuoss relation¹¹ $K_0 = 4\pi L d^3/3000$ which, taking $d = 7 \text{ \AA}$ as a reasonable parameter, gives $K_0 = 0.87$, namely, a quantity of the order of unity. In fact, $K_0 = 1$ has been the numerical value retained here.

Plots of S and P vs $f(\theta)$ for $\text{Li}^+ + \text{EG3}$ are given in Figure 4, parts A and B, respectively (supplementary material). Linear regression of S vs $f(\theta)$ gives a determination coefficient $r_1^2 = 0.85$, an intercept $I_1 = k_{-1} + k_2 + k_{-2} = 4.9 \times 10^8$, and a slope $S_1 = k_1 K_0 = 1.68 \times 10^9$. Linear regression of P vs $f(\theta)$ gives a determination coefficient $r_{II}^2 = 0.78$, an intercept $I_{II} = k_{-1} k_{-2} = 1.83 \times 10^{16}$, and a slope $S_{II} = k_1 K_0 (k_2 + k_{-2}) = 3.40 \times 10^{17}$.

From S_{II}/S_1 one calculates $k_2 + k_{-2}$; then $I_1 - (S_{II}/S_1) = k_{-1}$. Finally, $I_{II}/k_{-1} = k_{-2}$, which gives in turn $k_2 = S_{II}/S_1 - k_{-2}$.

Table II gives the rate constants calculated from the above sequence together with the average values of the equilibrium constants $K_1 = k_1/k_{-1}$ and $K_2 = k_2/k_{-2}$ as well as the overall

TABLE I: Ultrasonic Parameters and Sound Velocity (for LiClO₄ + EG3 and for LiClO₄ + EG4 at Molar Ratio *R* = 1 in Acetonitrile at 25 °C) for All the Concentrations Investigated^a

Ligand: EG3							
<i>C</i> _{LiClO₄} , M	<i>C</i> _{EG} , M	10 ⁵ <i>μ</i> _I	<i>f</i> _I , MHz	10 ⁵ <i>μ</i> _{II}	<i>f</i> _{II} , MHz	10 ¹⁷ <i>B</i> , cm ⁻¹ s ⁻²	10 ⁻⁵ <i>u</i> , cm s ⁻¹
0.026	0.026	110	75	110	7	57.5	1.287
0.050	0.050	140	85	150	9	57.5	1.294
0.10	0.10	180	80	180	13	58.0	1.286
0.20	0.20	300	100	270	18	55.5	1.287
0.30	0.30	430	95	290	14	56.0	1.297
0.40	0.40	520	100	270	20	56.0	1.300
0.50	0.50	560	100	300	16	56.0	1.308
0.75	0.75	750	100	340	16	58.0	1.317
1.0	1.0	878	120	326	20	67.0	1.331
Ligand: EG4							
<i>C</i> _{LiClO₄} , M	<i>C</i> _{EG} , M	10 ⁵ <i>μ</i> _I	<i>f</i> _I , MHz	10 ⁵ <i>μ</i> _{II}	<i>f</i> _{II} , MHz	10 ¹⁷ <i>B</i> , cm ⁻¹ s ⁻²	10 ⁻⁵ <i>u</i> , cm s ⁻¹
0.032	0.032	40	85	83	6	63.5	1.278
0.060	0.060	45	90	105	8	61.5	1.280
0.080	0.080	130	110	125	9	58.5	1.286
0.10	0.10	160	110	150	14	59	1.300
0.20	0.21	260	120	255	15	57	1.291
0.32	0.32	355	130	300	17	57	1.301
0.40	0.40	365	140	341	18	58	1.305
0.50	0.50	425	145	317	19	63.5	1.308
0.65	0.65	485	135	290	19	58	1.308
0.80	0.80	850	150	290	22	64	1.327
1.00	1.00	1000	155	340	20	60	1.319
<i>C</i> _{LiCF₃SO₃} , M	<i>C</i> _{EG₃} , M	10 ⁵ <i>μ</i> _I	<i>f</i> _I , MHz	10 ⁵ <i>μ</i> _{II}	<i>f</i> _{II} , MHz	10 ¹⁷ <i>B</i> , cm ⁻¹ s ⁻²	10 ⁻⁵ <i>u</i> , cm s ⁻¹
0.85	0.85	1300	160	500	17	68	1.277
0.60 ₅	0.60	760	150	541	18	67	1.267
0.46	0.46	650	130	450	16	67	1.276
0.30 ₃	0.30 ₅	443	120	420	15	65	1.272
0.10 ₃	0.10 ₅	266	110	295	11	62	1.275
0.30		350	95	270	14	57	1.271
Salt = LiAsF ₆ , Ligand = EG3							
<i>C</i> _{LiAsF₆} , M	<i>C</i> _{EG₃} , M	10 ⁵ <i>μ</i> _I	<i>f</i> _I , MHz	10 ⁵ <i>μ</i> _{II}	<i>f</i> _{II} , MHz	10 ¹⁷ <i>B</i> , cm ⁻¹ s ⁻²	10 ⁻⁵ <i>u</i> , cm s ⁻¹
1.00	1.00	500	170	600	30	62	1.267
0.75	0.75	350	155	468	26	61	1.263
0.60	0.60	450	150	375	20	58	1.261
0.44	0.45	280	123	360	19	57	1.264
0.31	0.30	280	120	310	16	58	1.263
0.11	0.11	253	120	170	12	57	1.280

^aThe parameters μ_I and μ_{II} are affected by an average error of $\pm 10\%$; the relaxation frequencies f_I and f_{II} by an average error of $\pm 10\%$. B is uncertain to within $\pm 1 \times 10^{-17}$ cm⁻¹ s⁻², whereas the experimental average error in the sound velocities corresponds to $\pm 0.5\%$.

average equilibrium constant $K_\Sigma = K_0(1 + K_1 + K_1K_2)$. Notice that $K_\Sigma = 20$ (instead of the value of $K_\Sigma = 50$ determined by NMR). The factor of 2.5 is neither meaningful nor significant, considering the large errors in K_1 and K_2 obtained from ratios of rate constants, and the distributed errors involved (Table II).

For Li⁺ and EG4, plots of S and P vs $f(\theta)$ are given in parts A and B of Figure 5, respectively (supplementary material). Linear regression of S vs $f(\theta)$ gives $r^2 = 0.91$, $I_I = 5.3_9 \times 10^8$, and $S_I = 4.47 \times 10^9$. Linear regression of P vs $f(\theta)$ gives $r^2 = 0.94$, $I_{II} = 6.9_7 \times 10^{15}$, and $S_{II} = 9.4_6 \times 10^{17}$.

The same sequence of calculations as done above for EG3 gives the rate constants k_1 , k_{-1} , k_2 , and k_{-2} , the equilibrium constants K_1 and K_2 , and an overall formation constant $K_\Sigma = 138$ which is close (given the large experimental error) to the value determined by NMR, namely, $K_\Sigma = 150$. Table II collects all the above calculated parameters.

Comparison between the rate constants and equilibrium constants for the complexation of Li⁺ with EG3 and for Li⁺ with EG4 reveals that all the rate constants are within a factor of about 3. The differences, however, lead to K_1 being a factor of 2 and to K_2 being a factor of 4 larger for Li⁺ + EG4 and eventually to K_Σ being larger for Li⁺ + EG4 in acetonitrile.

Physically, it appears that a flexible acyclic ligand with five binding oxygens such as EG4 more effectively complexes Li⁺ than the corresponding EG3 ligand with four binding oxygens. This is in contrast to the crown ethers, where 12C4 is expected to prevail over 15C5 when binding Li⁺ in terms of affinity expressed by K_Σ . In the crown case, however, one must consider factors such as the

TABLE II: Rate Constants and Equilibrium Constants in Acetonitrile for the Complexation of LiClO₄ with the Ligands EG3, EG4, and TG3 at 25 °C

	EG3	EG4	TG3 ^a
k_1 , s ⁻¹	$(1.7 \pm 0.3) \times 10^9$	$(4.5 \pm 0.4) \times 10^9$	4.9×10^8
k_{-1} , s ⁻¹	$(3.0 \pm 1.4) \times 10^8$	$(3.3 \pm 1.5) \times 10^8$	1.4×10^8
K_1	5.7 ± 3.5	13.6 ± 7.4	3.5
k_2 , s ⁻¹	$(1.4 \pm 1.6) \times 10^8$	$(1.9 \pm 0.4) \times 10^8$	1.2×10^{8b}
k_{-2} , s ⁻¹	$(0.6 \pm 1.1) \times 10^8$	$(2.1 \pm 0.7) \times 10^7$	9×10^6
K_2	2.3 ± 6.6	9.1 ± 5.1	13
K_0^c	1	1	1
K_Σ	20 ± 49	138 ± 149	50

^aData from ref 3. ^bThe figure $k_2 = 1.2 \times 10^7$ reported in ref 3 is a misprint. ^cEstimated from the relation $K_0 = 4\pi Ld^3/3000$, with $d \approx 7 \times 10^{-8}$ cm.

cavity size of the macrocycle 12C4 with respect to 15C5. For instance, in methanol Na⁺ binds 15C5 with a K_Σ larger by a factor of ~ 40 with respect to 12C4.¹² The radius of Na⁺, $r_{Na^+} = 1.0_2$ Å, is closer to that of the cavity of 15C5, $r_{15C5} = 0.85$ Å, than to the cavity radius of 12C4, $r_{12C4} = 0.6-0.75$.¹³ It is also of interest to compare the rate constants and equilibrium constants of Li⁺ + EG3 with the corresponding values for the system Li⁺ + triglyme which has the same chemical structure as EG3 but with the two -OH groups substituted by two methoxy groups, -OCH₃. Table II reports these literature data³ for Li⁺ + triglyme. The comparison reveals that all the constants are within a factor of 3 with the exception of k_{-2} , which is a factor of 7 smaller for

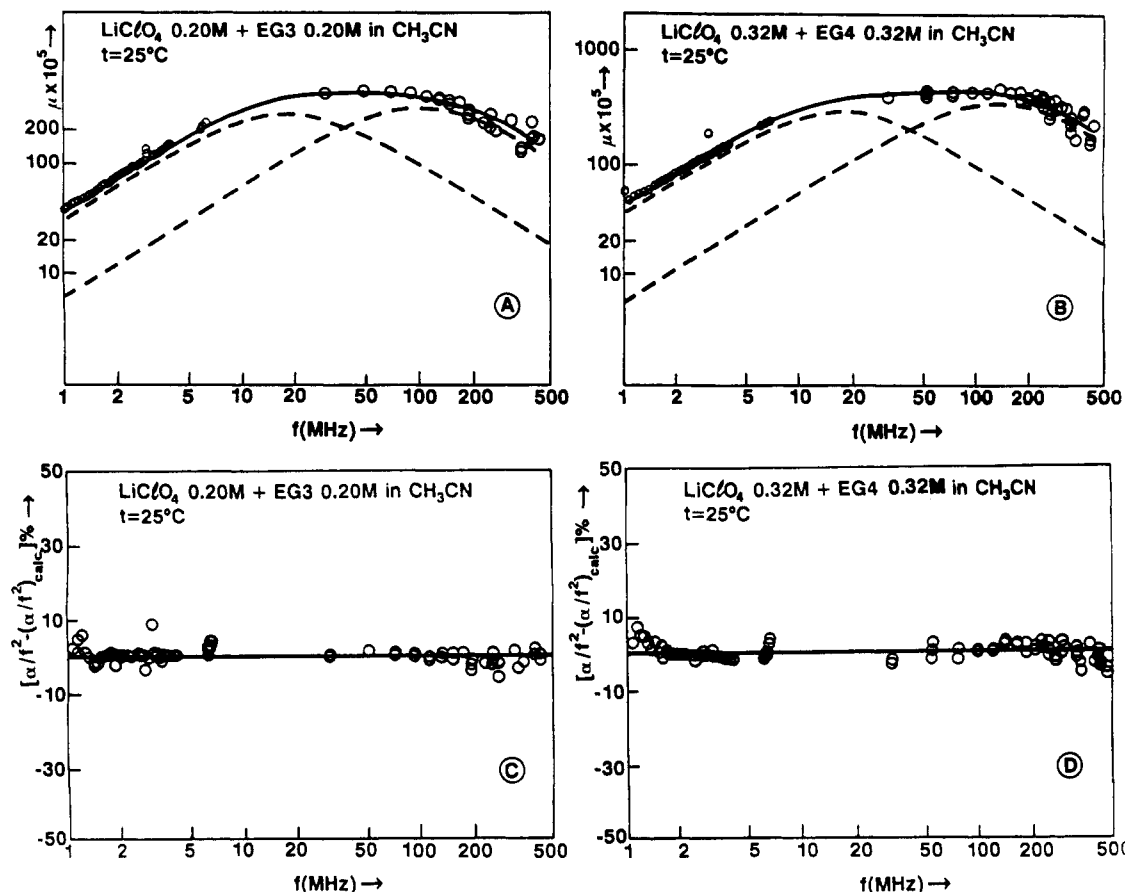


Figure 3. (A) Representative ultrasonic relaxation spectrum, in the form of the excess sound absorption per wavelength μ vs the frequency f , for $\text{LiClO}_4 + \text{EG3}$ at molar ratio $R = [\text{EG3}]/[\text{LiClO}_4] = 1$ in acetonitrile at 25°C . (B) Representative ultrasonic relaxation spectrum for $\text{LiClO}_4 + \text{EG4}$ at $R = 1$ in acetonitrile at 25°C . (C) Deviational plot of $[(\alpha/f^2) - (\alpha/f^2)_{\text{calc}}] \%$ vs the frequency f for $\text{LiClO}_4 + \text{EG3}$ in acetonitrile. Same data as for Figure 3A. (D) Deviational plot of $[(\alpha/f^2) - (\alpha/f^2)_{\text{calc}}] \%$ vs the frequency f for $\text{LiClO}_4 + \text{EG4}$ in acetonitrile. Same data as for Figure 3B.

Li^+ + triglyme leading to the conclusion that $K_2(\text{Li}^+ + \text{triglyme}) > K_2(\text{Li}^+ + \text{EG3})$.

To calculate the isentropic volume change for the normal modes I and II of the two observed processes, we require the two expressions¹⁴

$$\mu_I = \frac{\pi}{2\beta_s} \frac{\Delta V_I^2}{RT} \left[\frac{1}{\frac{1}{2}C_0 + C_1} + \frac{1}{C_2} \right]^{-1} = \frac{\pi}{2\beta_s} \frac{\Delta V_I^2}{RT} \Gamma_{I1}^{-1}$$

$$\mu_{II} = \frac{\pi}{2\beta_s} \frac{\Delta V_{II}^2}{RT} \left[\frac{1}{C_1 + C_2} + \frac{1}{C_3} \right]^{-1} = \frac{\pi}{2\beta_s} \frac{\Delta V_{II}^2}{RT} \Gamma_{II}^{-2} \quad (4)$$

Thus one can calculate ΔV_I and ΔV_{II} if one knows the isentropic compressibility $\beta_s = (\rho u^2)^{-1}$ along with $\rho = 0.777 \text{ g/cm}^3$, the density of the solution (taken to be about equal to that of the solvent), and u the sound velocity of the solutions. One must also calculate the concentration of the various species, here denoted by $C_0 = [\text{Li}^+] = [\text{EG}]$, $C_1 = [\text{Li}^+ \cdots \text{EG}]$, $C_2 = [\text{Li}^+ \text{EG}]$, and $C_3 = [(\text{Li}^+ \text{EG})_2]$.

To this end we have used the following relations for the $\text{Li}^+ + \text{EG3}$ system:

$$K_2 = 20 = \frac{C_1 + C_2 + C_3}{C_0^2} = \frac{C - C_0}{C_0^2}$$

$$K_0 = 1 = C_1/C_0^2$$

$$K_1 = 5.7 = C_2/C_1$$

$$K_2 = 2.3 = C_3/C_2$$

The value of $K_2 = 20$ had to be used in order to maintain internal consistency and because of the need for the values of K_1 and K_2 that are otherwise unknown. Parts A and B of Figure 6 (supplementary material) give μ_I and μ_{II} vs Γ_I^{-1} and Γ_{II}^{-1} , respectively. The plots are not linear preventing any calculations of $d\mu_I/d\Gamma_I^{-1}$

and of $d\mu_{II}/d\Gamma_{II}^{-1}$ and hence of ΔV_I and ΔV_{II} . The reason that the plots are not linear could be either the use of $K_2 = 20$ or a competition involving ClO_4^- in the complexation process (see below).

The situation with the system $\text{Li}^+ + \text{EG4}$ is much better. The same calculation run with $K_2 = 138$, $K_0 = 1$, $K_1 = 13.6$, and $K_2 = 9.1$ instead of $K_2 = 150$, for the same reasons noted above for $\text{Li}^+ + \text{EG3}$, leads to Figure 7. Linear regression of μ_I vs Γ_I^{-1} giving 50% statistical weight to the origin yields $r^2 = 0.96$, $I_1 = -4.9 \times 10^{-5}$, and $S_1 = 288$ from which one calculates

$$\Delta V_I = \left(\frac{2\beta_s RT}{\pi} \frac{d\mu_I}{d\Gamma_I^{-1}} \right)^{1/2} = 18.6 \text{ cm}^3/\text{mol} \quad (5)$$

with $\beta_s = (\rho u^2)^{-1} = 76.1 \times 10^{-12} \text{ dyn}^{-1} \text{ cm}^2$, the average compressibility of the solutions ($\bar{u} = 1.30 \times 10^5 \text{ cm s}^{-1}$). Linear regression is applied to the first four points of Figure 7B before the deviation from linearity occurs, probably due to anion effects.³ Giving 50% statistical weight to the origin, this yields $r^2 = 0.94$, $I_{II} = 7.5 \times 10^{-5}$, and $S_{II} = 215$ from which one calculates

$$\Delta V_{II} = \left[\frac{2\beta_s RT}{\pi} \frac{d\mu_{II}}{d\Gamma_{II}^{-1}} \right] = 16.1 \text{ cm}^3/\text{mol}$$

The value of ΔV_I is smaller by a factor of about 2 than the value for $\text{Li}^+ + \text{triglyme}$ of $\Delta V_I = 34.2 \text{ cm}^3/\text{mol}$. On the other hand, the value of ΔV_{II} is similar to that for $\text{Li}^+ + \text{triglyme}$ of $\Delta V_{II} = 13.4 \text{ cm}^3/\text{mol}$. Since both the introduction of the two $-\text{OH}$ groups in lieu of $-\text{OCH}_3$ groups and the addition of one $(-\text{CH}_2\text{CH}_2\text{O}-)$ unit differentiate EG4 from triglyme, comparisons are difficult. It is unfortunate that no ΔV_I or ΔV_{II} calculation is feasible for $\text{Li}^+ + \text{EG3}$ systems, as shown above.

Infrared Data: Anion Effect. The saturation effect of μ_{II} vs Γ_{II}^{-1} shown in Figures 6B and 7B had already been reported³ for

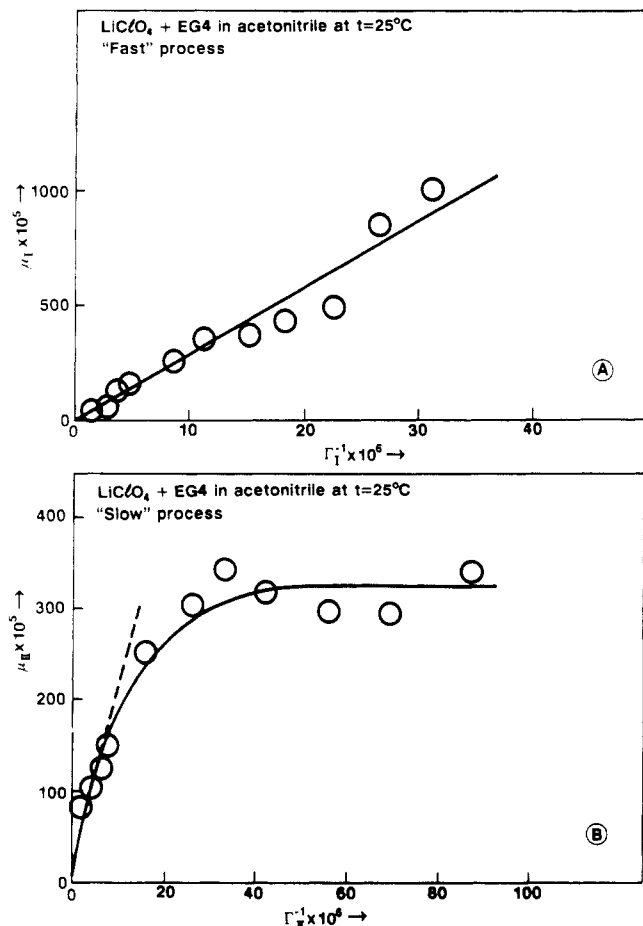


Figure 7. (A) μ_I vs Γ_I^{-1} for LiClO₄ + EG4 in acetonitrile at 25 °C. (B) μ_{II} vs Γ_{II}^{-1} for LiClO₄ + EG4 in acetonitrile at 25 °C.

the system LiClO₄ + triglyme in acetonitrile at 25 °C. This effect varied with the nature of the anion, and it was attributed to the anion competing with the glyme for the first coordination sphere positions around Li⁺. The same interpretation is given here for the trends in Figures 6B and 7B. We wished, however, to have an independent experimental confirmation of this interpretation. To this end we have recorded infrared spectra of the $\bar{\nu}_4$ vibrational mode of the ClO₄⁻ ion in the spectral region around ~ 625 cm⁻¹. Figure 8A reports the spectrum of 1.0 M LiClO₄ showing clearly that the spectral envelope can be reproduced by the sum of two Gaussian-Lorentzian product functions¹⁵

$$A_j = A_j^0 \left[\exp\left(-\frac{(\bar{\nu} - \bar{\nu}_j^0)^2}{2\sigma^2}\right) \right] \left[1 + \frac{(\bar{\nu} - \bar{\nu}_j^0)^2}{\sigma^2} \right]^{-1} \quad (6)$$

with $\sigma = (\Delta\bar{\nu}_j)_{1/2}/1.46$ denoting the standard error and $(\Delta\bar{\nu}_j)_{1/2}$ the width of each band centered at the wavenumber $\bar{\nu}_j$ and measured at half-maximum absorbance $A_j^0/2$ for that band. The fit of the spectral envelope by the sum of Gaussian-Lorentzian product functions (eq 6) has been done by a computer graphic method allowing for iterative changes of the parameters A_j^0 , $\bar{\nu}_j^0$, and $(\Delta\bar{\nu}_j)_{1/2}$ for each band up to an optimum fit by minimizing the $|A - A_{\text{calc}}|$ for the total spectral envelope. The choice of the number of Gaussian-Lorentzian product functions (eq 6) necessary to reproduce each spectral envelope was dictated by evidence of the presence of asymmetry, shoulders or multiple peaks in the spectra studied. The existence of a satellite band at $\bar{\nu} \approx 632$ cm⁻¹ for 1 M LiClO₄ in acetonitrile is ascribed to a contact ion pair, as done previously for other solvent systems dissolving LiClO₄.¹⁶ In 2MeTHF, the band appeared, however, at $\bar{\nu} = 638$ cm⁻¹. Figure 8, parts B and C, show the infrared spectrum in the same wavenumber region for the system 1.0 M LiClO₄ + 1.0 M EG3 and 1.0 M LiClO₄ + 1.0 M EG4 in acetonitrile. Again the spectral envelope can be interpreted by the sum of two Gaussian-Lorentzian product functions, but the amplitude of the

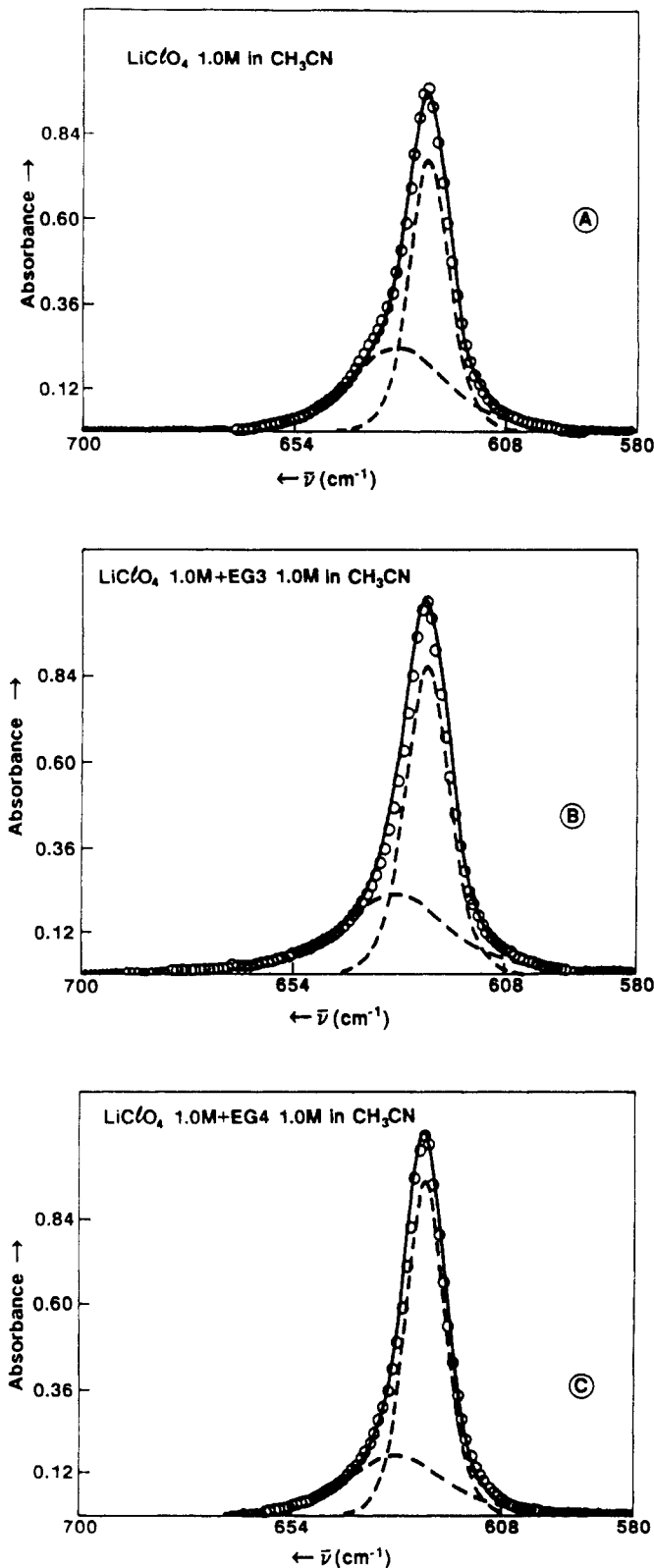


Figure 8. (A) Infrared spectrum of 1.0 M LiClO₄ in acetonitrile expressed in absorbance vs wavenumber $\bar{\nu}$. The spectral region for the $\bar{\nu}_4$ mode of ClO₄⁻ is depicted. The dashed line expresses the contribution of eq 6 for each band component. (B) Infrared spectrum for the $\bar{\nu}_4$ mode of ClO₄⁻ for the system 1.0 M LiClO₄ + 1.0 M EG3 in acetonitrile. (C) Infrared spectrum for the $\bar{\nu}_4$ mode of ClO₄⁻ for the system 1.0 M LiClO₄ + 1.0 M EG4 in acetonitrile.

satellite band appears reduced with respect to 1.0 M LiClO₄ as reported in Table III in the form of the normalized A_{632}^0/I absorbances. The reduction appears to be larger for EG4 than for EG3 reflecting both the larger K_2 of EG4 and the better ability of the pentadentate ligand to segregate ClO₄⁻ out of contact with Li⁺.

TABLE III: Infrared Parameters A_j° , ν_j° , $(\Delta\nu_j)_{1/2}$, Cell Length l , and Normalized Maximum Absorbance (A_j°/l) for the Band Components of the Spectra of 1 M LiClO₄ and of 1 M LiClO₄ Added to the Acyclic Ligands EG3, EG4, TG3, and TG4, and to the Cyclic Ligands 12C4 and 15C5 at $C = 1.0$ M, Each in Acetonitrile^a

A°_{625}	ν°_{625}	$\Delta\nu_{1/2}$	A°_{632}	ν°_{632}	$\Delta\nu_{1/2}$	A°_{625}/l	A°_{632}/l
Ligand = None, $l = 0.00478$ cm							
0.78	625	10	0.24	632	25	163	50.2
Ligand = EG3, $l = 0.00530_3$ cm							
0.87	625	11	0.23	632	27	164	43.3
Ligand = EG4, $l = 0.00478$ cm							
0.95	625	10	0.17	631.5	25	199	35.6
Ligand = TG3, $l = 0.0051$ cm							
0.90	625	10.5	0.13	633	24	177	25.5
Ligand = TG4, $l = 0.0051$ cm							
1.05	624.5	10.5	0.12	632	24	206	23.5
Ligand = 12C4, $l = 0.00505$ cm							
1.05	624.5	9	0.165	632	25	208	32.7
Ligand = 15C5, $l = 0.00503$ cm							
1.15	624.5	9.5	0.135	630	25	229	26.8

^aThe spectral region studied corresponds to the ν_4 normal mode of ClO₄⁻.

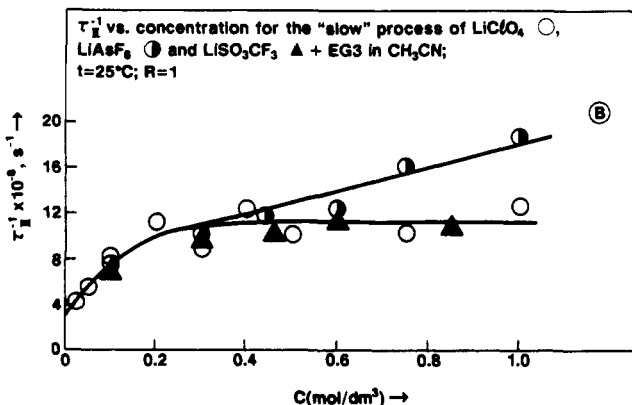
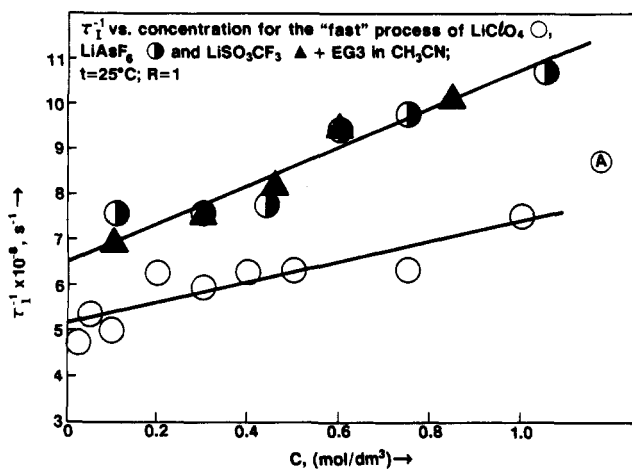


Figure 10. (A) τ_1^{-1} vs concentration for the fast process of LiClO₄ ○, LiAsF₆ ●, LiSO₃CF₃ ▲ + EG3 in CH₃CN; at 25 °C; molar ratio $R = 1$. (B) τ_{II}^{-1} vs concentration for the slow process of LiClO₄ ○, LiAsF₆ ●, and LiSO₃CF₃ ▲ + EG3 in CH₃CN; at 25 °C; molar ratio $R = 1$.

Figures 9, parts A and B (supplementary material) present the same spectrum for the systems 1.0 M LiClO₄ + 1.0 M triglyme (TG3) and 1.0 M LiClO₄ + 1.0 M tetraglyme (TG4), respectively, in acetonitrile. The spectra can also be interpreted by the sum of two Gaussian-Lorentzian product functions. Table III reports the parameters A_j° , ν_j° , $(\Delta\nu_j)_{1/2}$ for each band of the above fitted spectra, the thickness l of the infrared cell, and the normalized maximum absorbances per unit cell length A_j°/l for each band. The normalized amplitudes (A°_{632}/l) appear now reduced by a factor of about 2 with respect to the normalized amplitude (A°_{632}/l) of the satellite band of LiClO₄ 1.0 M.

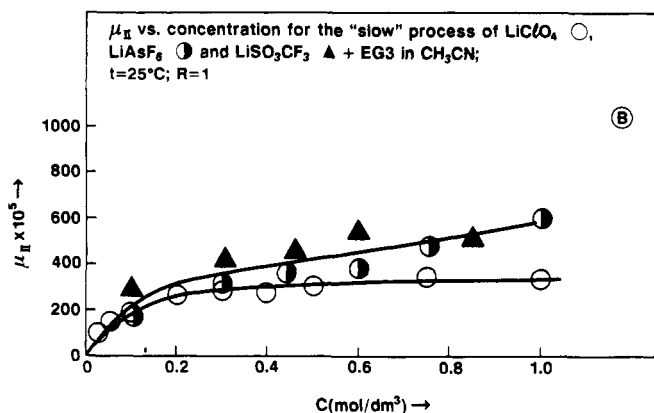
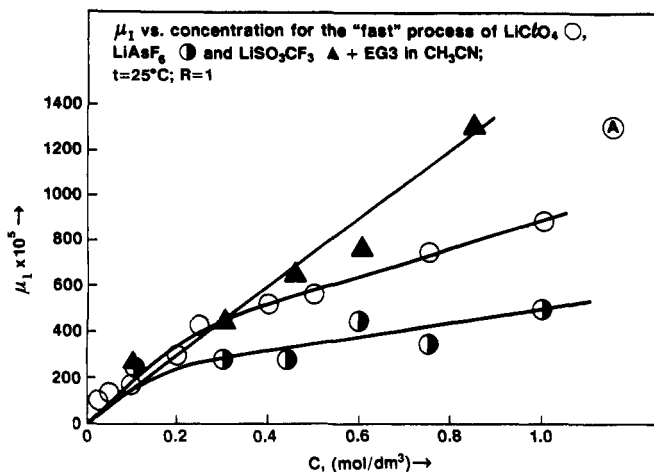


Figure 11. (A) μ_1 vs concentration for the fast process of LiClO₄ ○, LiAsF₆ ●, and LiSO₃CF₃ ▲ + EG3 in CH₃CN; at 25 °C; molar ratio $R = 1$. (B) μ_{II} vs concentration for the slow process of LiClO₄ ○, LiAsF₆ ●, and LiSO₃CF₃ ▲ + EG3 in CH₃CN; at 25 °C; molar ratio $R = 1$.

Figure 9, parts C and D (supplementary material) are the infrared spectra of the systems 1.0 M LiClO₄ + the cyclic macrocycles 1.0 M 12C4 and 1.0 M 15C5 in acetonitrile. Again these spectral envelopes may be interpreted by the sum of two Gaussian-Lorentzian bands, but, whereas the normalized A°_{632}/l for 15C5 is comparable to the value for TG4, the value of A°_{632}/l for 12C4 is larger. Perhaps the decrease in the bands reflects the steric ability of the etheral ligands to segregate Li⁺ from contacting ClO₄⁻ in addition to the complexation of Li⁺ with the etheral ligands. This would explain the larger A°_{632}/l value for 12C4 with respect to that for 15C5 and the persistences of a satellite species for ClO₄⁻ in the presence of the macrocyclic ligands, which presumably have larger formation constants with the Li⁺ than do the acyclic ethers. Solid-state X-ray crystallographic data¹⁷ for RbSCN + dibenzo-18C6 show that Rb⁺ is complexed by the macrocyclic ether through the oxygen atoms and lies slightly out of the plane of the crown ether. Also, Rb⁺ is coordinated with the nitrogen end of the anion pointing toward Rb⁺, the anion being normally oriented with respect to the crown ether. The complete system looks like an umbrella blown inside out by a gust of wind.

Anion Effect: Nature of the Anion. In a previous paper,³ it was pointed out that LiClO₄ and LiAsF₆ complexing triglyme in CH₃CN yielded different excess sound absorptions per wavelength μ_1 and μ_{II} .

Ultrasonic spectra of LiAsF₆ and of lithium triflate LiSO₃CF₃ in molar ratio $R = 1$ with EG3 in the solvent acetonitrile at 25 °C have been recorded. The spectra can be interpreted by the sum of two Debye relaxation processes. Table I reports the parameters $f_1, f_{II}, \mu_1, \mu_{II}, B$, and the sound velocity u for the above two systems at the concentrations investigated in CH₃CN at 25 °C. An effect specific to the anion is visible in both plots of τ_1^{-1} vs concentration C (Figure 10A) and τ_{II}^{-1} vs concentration C (Figure 10B). In particular, this effect is present over the entire concentration range for the "fast" process characterized by τ_1^{-1} ,

TABLE IV: Infrared Parameters A° , $\bar{\nu}^\circ$, $(\Delta\bar{\nu}_{1/2})$, Cell Length l for the Band Components of the Spectra of LiX (X = AsF₆⁻, CF₃SO₃⁻) and of LiX Added of the Acyclic Ligands EG3 and EG4 in Acetonitrile

$X = \text{AsF}_6^-, n = 3$							
C_{LiAsF_6}	C_{EG_n}	A°_{750}	$\bar{\nu}^\circ_{750}$	$(\Delta\bar{\nu}_{1/2})_{750}$	A°_{704}	$\bar{\nu}^\circ_{704}$	
0.40 ₀	0.40 ₂	0.11	750	18	1.88	703.7	
0.30 ₀	0.30 ₀	0.125	750	18	1.49	703.7	
0.20 ₀	0.20 ₀	0.26	749	18	2.12	703.5	
0.15 ₂	0.16 ₀	0.24	749.5	18	1.46	703.5	
0.10 ₁	0.099	0.25	749.5	17	1.02	703.5	
0.075 ₇	0.076 ₁	0.26	749.5	16.5	0.78 ₂	703.7	
0.050 ₅	0.049	0.28	749	17	0.54	703.7	
0.028 ₆	0.032	0.26	749.5	17	0.29 ₅	703.7	
C_{LiAsF_6}	$(\Delta\bar{\nu}_{1/2})_{704}$	$10^3 l_{\text{cell}}, \text{cm}$	C_{LiAsF_6}	$(\Delta\bar{\nu}_{1/2})_{704}$	$10^3 l_{\text{cell}}, \text{cm}$		
0.40 ₀	12.3	2.27	0.10 ₁	11.5	4.7 ₃		
0.30 ₀	11.5	2.41	0.075 ₇	10.5	4.7 ₃		
0.20 ₀	11.5	5.0 ₀	0.050 ₅	11.8	5.0 ₃		
0.15 ₂	11.5	4.6 ₂	0.028 ₆	10.5	4.70		
$X = \text{AsF}_6^-, n = 4$							
C_{LiAsF_6}	EG_n	A°_{750}	$\bar{\nu}^\circ_{750}$	$(\Delta\bar{\nu}_{1/2})_{750}$	A°_{704}	$\bar{\nu}^\circ_{704}$	
0.400	0.400	0.11	749.5	17	2.35	703.7	
0.300	0.301	0.11	749.5	17	1.58	703.7	
0.201	0.203	0.11	749.7	17	0.95	704	
0.156	0.155	0.12	749.5	17	0.81	703.7	
0.102	0.101	0.25	750.2	17	1.02	705	
0.050	0.052 ₄	0.24	750.2	17	0.49	705	
C_{LiAsF_6}	$(\Delta\bar{\nu}_{1/2})_{704}$	$10^3 l_{\text{cell}}, \text{cm}$	C_{LiAsF_6}	$(\Delta\bar{\nu}_{1/2})_{704}$	$10^3 l_{\text{cell}}, \text{cm}$		
0.400	12	2.54	0.156	12	2.44		
0.300	12	2.7 ₀	0.102	11	4.6 ₃		
0.201	11.5	2.17	0.050	10.8	4.38		
$X = \text{AsF}_6^-$							
C_{LiAsF_6}	C_{EG_n}	A°_{750}	$\bar{\nu}^\circ_{750}$	$(\Delta\bar{\nu}_{1/2})_{750}$	A°_{704}	$\bar{\nu}^\circ_{704}$	
0.399		0.11	749.5	17	1.88	703.7	
0.300		0.11	749.5	17	1.45	703.7	
0.150		0.24	749.5	18	1.48	704	
C_{LiAsF_6}	$(\Delta\bar{\nu}_{1/2})_{704}$	$10^3 l_{\text{cell}}, \text{cm}$	C_{LiAsF_6}	$(\Delta\bar{\nu}_{1/2})_{704}$	$10^3 l_{\text{cell}}, \text{cm}$		
0.399	12.5	2.3 ₉	0.150	11.2	4.7 ₉		
0.300	11.5	2.1 ₀					
$X = \text{CF}_3\text{SO}_3^-, n = 3$							
C_{LiX}	C_{EG_n}	A°_{1300}	$\bar{\nu}^\circ_{1300}$	$(\Delta\bar{\nu}_{1/2})_{1300}$	A°_{1273}	$\bar{\nu}^\circ_{1273}$	
0.192		0.48	1299.5	15	0.39	1273	
0.174		0.44	1299.5	16	0.38	1273	
0.152		0.36	1299.5	17	0.32	1272.5	
0.126		0.29	1299.5	14	0.27 ₅	1273	
0.10 ₀		0.70	1299.5	14	0.78 ₅	1272.5	
0.074 ₅		0.54	1299.5	14.5	0.70	1272.5	
0.048 ₆		0.28	1299.5	14	0.50	1272.5	
0.0256		0.14	1299.5	14	0.33	1272.5	
0.130		0.09	1299.5	10	0.27	1272	
$(\Delta\bar{\nu}_{1/2})_{1273}$	A°_{1256}	$\bar{\nu}^\circ_{1256}$	$(\Delta\bar{\nu}_{1/2})_{1256}$	A°_{1227}	$\bar{\nu}^\circ_{1227}$	$(\Delta\bar{\nu}_{1/2})_{1227}$	$10^3 l_{\text{cell}}, \text{cm}$
17	0.42	1256	17	0.145	1227.5	11	3.02
17	0.39	1256	16.5	0.14	1227.5	12	3.01
17	0.31	1256.5	16	0.11	1227	13	3.01
16.5	0.27 ₅	1256.5	16	0.09	1227.5	10	3.01
15.5	0.69 ₅	1256.5	16	0.25	1227	11	10.6
16.5	0.57	1256	17.2	0.25	1227	13.5	10.6
15.5	0.32	1256.5	16.5	0.14	1227	11.5	10.6
15.5	0.19	1256.5	17.5	0.075	1225.5	12	10.6
14	0.13 ₅	1257	16.5	0.065	1225.5	11	10.6
$\text{LiSO}_2\text{CF}_3 + \text{EG3 in CH}_3\text{CN, X} = \text{CF}_3\text{SO}_3^-, n = 3$							
$C_{\text{LiCF}_3\text{SO}_3}$	C_{EG_3}	A°_{1296}	$\bar{\nu}^\circ_{1295}$	$(\Delta\bar{\nu}_{1/2})_{1296}$	A°_{1272}	$\bar{\nu}^\circ_{1272}$	
0.202	0.203	0.25	1295	21	0.49	1271	
0.174	0.178	0.205	1295	20	0.43	1271.5	
0.152	0.152	0.19	1295.5	21	0.38 ₅	1272	
0.124	0.125	0.13	1295.5	20	0.33	1272	
0.100	0.105	0.26	1297.5	17	0.79	1271.7	
0.0775	0.0737	0.31	1296	21	0.90	1272	
0.0464	0.0445	0.128	1297	15	0.58	1271.7	
0.0132	0.0127	0.046	1297	19	0.25	1272	
0.0267	0.0330	0.080	1296	20	0.40	1272	

TABLE IV (Continued)

$(\Delta\bar{\nu}_{1/2})_{1272}$	A°_{1254}	$\bar{\nu}^{\circ}_{1254}$	$(\Delta\bar{\nu}_{1/2})_{1254}$	A°_{1226}	$\bar{\nu}^{\circ}_{1226}$	$(\Delta\bar{\nu}_{1/2})_{1226}$	$10^3 I_{\text{cell}}$
18	0.26	1253	21	0.17	1226	12	3.01
17	0.23 ₅	1253.5	22	0.16	1225.5	12	3.00 ₆
18	0.21 ₅	1254	23	0.19	1225.5	12	3.00 ₅
17	0.15	1254.5	22	0.10	1225.5	12	3.02
17	0.31	1254	18	0.20	1226	12	10.5 ₇
17	0.38 ₅	1254	22	0.24	1225.5	12.5	3.02
16	0.173	1254.5	19	0.13	1226	11.5	10.5 ₇
17	0.079	1255	22	0.05	1225.5	13	10.5 ₇
16	0.135	1255	22	0.08	1225.5	12	10.5 ₇

X = CF₃SO₃⁻, n = 4

$C_{\text{LiCF}_3\text{SO}_3}$	C_{EG4}	A°_{1296}	$\bar{\nu}^{\circ}_{1296}$	$(\Delta\bar{\nu}_{1/2})_{1296}$	A°_{1272}	$\bar{\nu}^{\circ}_{1272}$
0.10	0.10 ₆	0.315	1295.5	18	1.11	1272

$(\Delta\bar{\nu}_{1/2})_{1272}$	A°_{1254}	$\bar{\nu}^{\circ}_{1254}$	$(\Delta\bar{\nu}_{1/2})_{1254}$	A°_{1226}	$\bar{\nu}^{\circ}_{1226}$	$(\Delta\bar{\nu}_{1/2})_{1226}$	$10^3 I_{\text{cell}}$
17	0.30	1254	19	0.23	1226	12	10.57

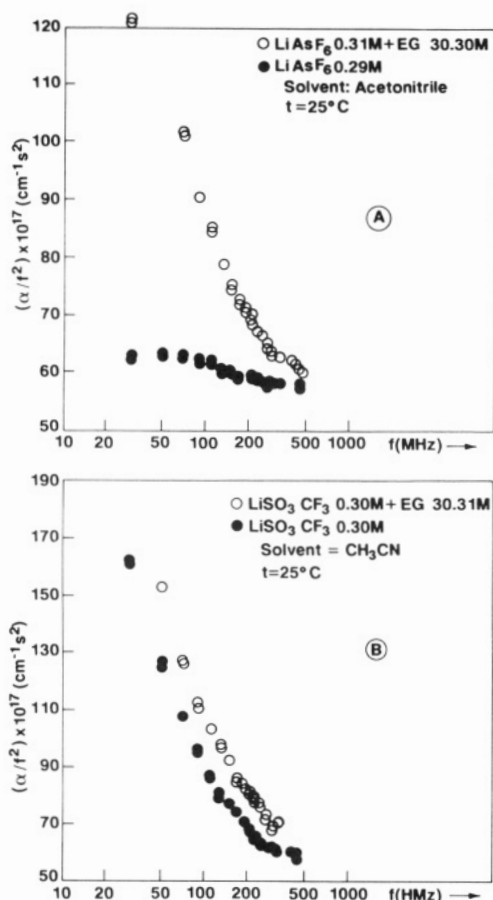


Figure 12. (A) α/f^2 vs frequency f for 0.31 M LiAsF₆ + 0.30 M EG3 ○, and 0.29 M LiAsF₆ ●, in CH₃CN at 25 °C. (B) (α/f^2) vs frequency f for 0.30 M LiSO₃CF₃ + 0.31 M EG3 ○ and 0.30 M LiSO₃CF₃ ● in CH₃CN at 25 °C.

but is present only for $C \geq 0.4$ M for the "slow" process characterized by τ_{II}^{-1} . Figure 11, parts A and B, depicts μ_1 and μ_{II} vs the concentration for the three electrolytes + EG3 at molar ratio $R = [\text{EG3}]/[\text{LiX}] = 1$ ($X^- = \text{ClO}_4^-, \text{AsF}_6^-, \text{CF}_3\text{SO}_3^-$). The same specificity with regard to the nature of the anion appears at $C \geq 0.2$ M. Evidently, the anion competes with EG3 for coordination sites around Li⁺. The two ligands, the anion and EG3 interfere also during the first "fast" step as shown by the specificity of τ_1^{-1} and μ_1 to the nature of the anion. In search of proofs of these statements, we have run the ultrasonic spectrum of LiAsF₆ 0.30 M in CH₃CN at 25 °C. A small ultrasonic relaxation centered at frequencies above 100 MHz is present for the electrolyte alone. (Ultrasonic spectra of 0.31 M LiAsF₆ + 0.30 M EG3 and of 0.30 M LiAsF₆ alone in CH₃CN at 25 °C are compared in Figure 12A. Both spectra are plotted as α/f^2 vs the frequency f .)

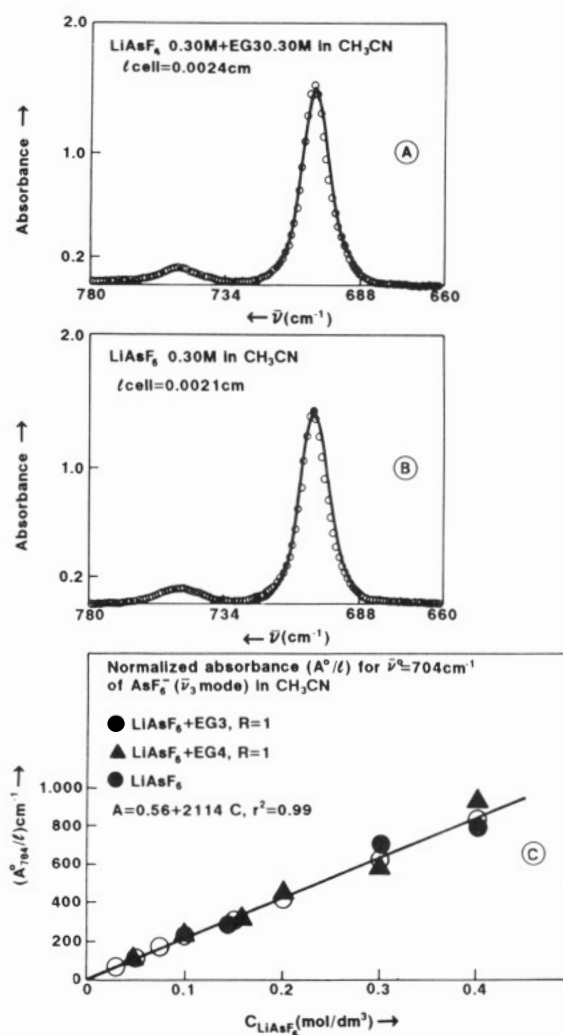


Figure 13. (A) Infrared spectrum: 0.30 M LiAsF₆ + 0.30 M EG3 in CH₃CN; $l_{\text{cell}} = 0.0024$ cm. The band centered at 750 cm⁻¹ belongs to the solvent. (B) IR spectrum: LiAsF₆ 0.30 M in CH₃CN; $l_{\text{cell}} = 0.0021$ cm. (C) Normalized absorbance per unit cell length A°/l for the ν_3 mode of AsF₆⁻ in CH₃CN. Systems: LiAsF₆ + EG3 at $R = 1$; LiAsF₆ + EG4 at $R = 1$.

Figure 12B shows the ultrasonic spectrum of 0.30 M lithium triflate in CH₃CN in the form of (α/f^2) vs f compared with that of 0.30 M lithium triflate + 0.30 M EG3 in CH₃CN at 25 °C. The two spectra are comparable putting into question the relative role of the ligand responsible for the relaxation process for the lithium triflate + EG3 system. This is a quite surprising result since LiSO₃CF₃ is widely used by polymer chemists in media of lower permittivity than CH₃CN (such as pure liquid polymers) in the expectation that the triflate anion does not interfere with the polymer chain in complexing Li⁺.

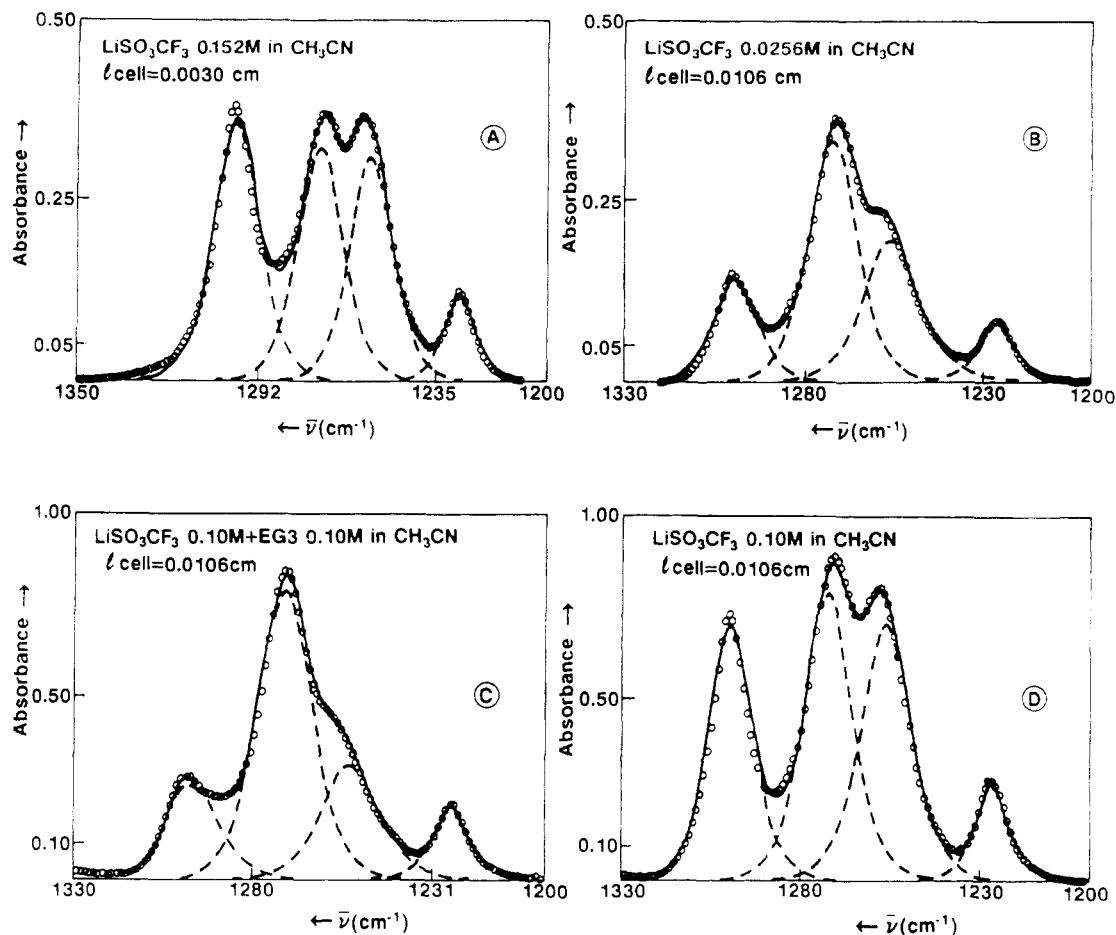


Figure 14. (A) IR spectrum: LiSO_3CF_3 0.15 M in CH_3CN $l_{\text{cell}} = 0.0030$ cm. (B) 0.0256 M LiSO_3CF_3 in CH_3CN ; $l_{\text{cell}} = 0.0106$ cm. (C) 0.10 M LiSO_3CF_3 + 0.10 M EG3 in CH_3CN $l_{\text{cell}} = 0.0106$ cm. (D) 0.10 M LiSO_3CF_3 in CH_3CN ; $l_{\text{cell}} = 0.0106$ cm.

An extensive infrared investigation has been carried out, searching for a more direct structural proof of the competition between the anions and EG3 (or EG4) for a first coordination sphere site on Li^+ in CH_3CN . Figure 13A reports the $\bar{\nu}_3$ mode of vibration of the AsF_6^- ion in the 690–730- cm^{-1} wavenumber range for a representative $\text{LiAsF}_6 + \text{EG3}$ system at molar ratio $R = 1$ in CH_3CN . The band centered at $\bar{\nu}^0 \approx 750$ cm^{-1} belongs to the solvent. Figure 13B reports the same spectrum for the electrolyte LiAsF_6 alone in CH_3CN . No apparent alteration of the spectrum occurs because of the presence of EG3 (or EG4 in corresponding spectra). This confirms the ultrasonic results showing no effect due to the anion for $C \leq 0.40$ M, for the “slow” process, but only an effect present for the “fast” process (Figure 10B,A). Evidently, the vibrational spectra cannot distinguish noncontact effects ascribable to the AsF_6^- ion. Therefore only interactions leading to contact species will affect the $\bar{\nu}_3$ mode of the AsF_6^- ion. On the contrary, the ultrasonic relaxation spectrum monitors interference of outer-sphere AsF_6^- to the substitution of solvent around Li^+ by EG3 or EG4. The faster τ_1^{-1} for Li^+ when AsF_6^- is present may reflect an easier release of CH_3CN from the $\text{Li}(\text{CH}_3\text{CN})_{x-1}^+\text{AsF}_6^-$ ion pair compared to $\text{Li}^+(\text{CH}_3\text{CN})_x$.

Figure 13C reports the normalized (A^0/l) for unit cell length l for the bands of the AsF_6^- ion of the above systems. All the data fall on the same line within experimental error. Table IV reports the infrared parameters $\bar{\nu}^0$, A^0 , and $(\Delta\bar{\nu})_{1/2}$ according to the Gaussian-Lorentzian product functions (eq 6) used to interpret the $\bar{\nu}_3$ envelope of the AsF_6^- ion for these systems.

We then investigated the triflate ion, CF_3SO_3^- , for the LiSO_3CF_3 solutions in CH_3CN and for the $\text{LiSO}_3\text{CF}_3 + \text{EG3}$ solutions in CH_3CN at molar ratio $R = 1$. Figure 14A reports the spectral envelope of the CF_3SO_3^- ion for the system 0.152 M LiSO_3CF_3 in CH_3CN in the wavenumber region 1330–1200 cm^{-1} . Figure 14B reports the same spectral envelope for 0.0256 M LiSO_3CF_3 in CH_3CN . This region of the $-\text{SO}_3^-$ spectrum cor-

responds to the asymmetric SO_3 stretch. The spectral envelope can be interpreted by the sum of four Gaussian-Lorentzian bands (eq 6) centered around 1300, 1273, 1257, and 1227 cm^{-1} . From the figure, it is apparent that the bands at 1300 and 1257 cm^{-1} change with concentration faster than the others. This could be attributed to either these bands having a larger molar absorptivity or extinction coefficient or to the effect of Li^+ forming contact ion pairs as described below. Table IV reports all the infrared parameters A^0 , $\bar{\nu}^0$, and $(\Delta\bar{\nu})_{1/2}$ belonging to the bands of the spectral envelope according to the computer graphics fit. Figure 14C,D reports the same spectral region for the system $\text{LiSO}_3\text{CF}_3 + \text{EG3}$ at molar ratio = 1 at a concentration 0.105 M and for 0.10 M LiSO_3CF_3 . The effect of the addition of EG3 (which has no absorption band in this region of the spectrum) is to decrease dramatically the bands at ~ 1300 and at ~ 1257 cm^{-1} . This effect is equivalent to the one of diluting LiSO_3CF_3 , as shown in Figure 14A,B. Hence EG3 seems to be able to segregate partially Li^+ from contacting the sulfonate group of the triflate ion, showing that LiSO_3CF_3 in acetonitrile has extensive ion pairing. This confirms the ultrasonic results above. Figure 15A,B (supplementary material) reports the normalized A^0/l vs C for the four bands of the LiSO_3CF_3 and of $\text{LiSO}_3\text{CF}_3 + \text{EG3}$ at $R = 1$ in acetonitrile.

Conclusions

Substitution of both $-\text{OCH}_3$ groups of triglyme with $-\text{OH}$ groups of EG3 does not alter dramatically the kinetics of complexation of Li^+ with these ethereal ligands. The $-\text{OH}$ groups undoubtedly interact with Li^+ , as demonstrated by the IR spectra in the $-\text{OH}$ stretch region, shown in Figure 2. The spectra do not allow, however, a determination of whether this interaction is prevalent in the initial contact process, or when Li^+ is subsequently embedded in the ethereal coil of the ligand.

Addition of a $(-\text{CH}_2\text{CH}_2\text{O}-)$ moiety, as in EG4 contrasted with EG3, makes possible coordination of Li^+ ion by five instead of

four oxygen atoms. Both rate constants and equilibrium constants are altered by a factor of 3 or 4, the pentadentate ligand appearing to be favored over the tetradentate ligand (at variance with what is generally known for cyclic ligands such as the crown ethers, when complexed to Li^+).

The anion ClO_4^- seems to play a competitive role in the process of complexation of Li^+ by both EG3 and EG4 as reflected by the saturation observed in μ_{II} vs Γ_{II}^{-1} plots. The infrared spectra document the persistent contact of the anion with Li^+ at $C = 1.0$ M in the presence of all the acyclic and cyclic ligands studied so far in acetonitrile. Use of AsF_6^- and especially of CF_3SO_3^- anions shows the presence of a competitive interaction with EG3 for the first coordination sphere position of lithium ions. The "fast" process is affected over the entire concentration range, the "slow" process shows individual behavior above ~ 0.4 M, as far as τ_1^{-1} and τ_{II}^{-1} are concerned. The values of μ_1 and μ_{II} appear to be affected by the nature of the anion above $C \approx 0.2$ M.

The conclusion of this portion of the work is that in solvents of intermediate permittivity such as acetonitrile ($\epsilon_{25} = 36.0$) but of relatively low donor number ($\text{DN} = 14$), the anion plays a significant competitive role when Li^+ interacts with an acyclic polyether. The situation is bound to become worse in terms of anion competition in solvents of lower permittivity or by eliminating the solvent in pure polyether liquid solutions of permittivity of the order of 10.

Acknowledgment. We thank the National Science Foundation for support through Grant No. CHE 8822333.

Registry No. EG3, 112-27-6; EG4, 112-60-7; Li, 7439-93-2.

Supplementary Material Available: Plots of S and P vs $f(\theta)$ for $\text{LiClO}_4 + \text{EG3}$ in CH_3CN (Figure 4) and for $\text{LiClO}_4 + \text{EG4}$ in CH_3CN (Figure 5), μ_1 vs Γ_1^{-1} and μ_{II} vs Γ_{II}^{-1} for $\text{LiClO}_4 + \text{EG3}$ in CH_3CN (Figure 6), IR spectra of LiClO_4 with TG3, TG4, 12C4, and 15C5 in CH_3CN (Figure 9), normalized absorbances per unit optical path length vs concentrations for four IR bands

for LiSO_3CF_3 and $\text{LiSO}_3\text{CF}_3 + \text{EG3}$ in CH_3CN (Figure 15), and S and P derived from the mechanism of eq 2 in an Appendix (9 pages). Ordering information is given on any current masthead page.

References and Notes

- (1) *Basic Mechanisms in the Action of Lithium*; Emrich, H. M., Aldenhoff, J. B., Lux, H. D., Eds.; Excerpta Medica: Amsterdam, 1982.
- (2) Kaplan, M. L.; Reitman, E. A.; Holt, L. K.; Chandross, E. A. *Solid State Ionics* 1987, 25, 37.
- (3) Eschmann, J.; Strasser, J.; Xu, M.; Okamoto, Y.; Eyring, E. M.; Petrucci, S. *J. Phys. Chem.* 1990, 94, 3908.
- (4) Delsignore, M.; Maaser, H. E.; Petrucci, S. *J. Phys. Chem.* 1984, 88, 2405.
- (5) Farrow, M. M.; Olsen, S. L.; Purdie, N.; Eyring, E. M. *Rev. Sci. Instrum.* 1976, 47, 657.
- (6) Echegoyen, L.; Gokel, G. W.; Kim, S.; Eyring, E. M.; Petrucci, S. *J. Phys. Chem.* 1987, 91, 3854.
- (7) Sato, H.; Kusumoto, Y. *Chem. Lett.* 1978, 635.
- (8) For a review see: Farber, H.; Petrucci, S. *Ultrasonic Absorption Spectrometry*. In *The Chemical Physics of Solvation*; Dogonadze, R. R., et al., Eds.; Elsevier: Amsterdam, 1986; Part B, Chapter 9.
- (9) Eigen, M.; Winkler, R. In *Neurosciences, Second Study Program*; Schmidt, F. O., Ed.; Rockefeller University Press: New York, 1970; p 685.
- (10) Cobranchi, D. P.; Garland, B. A.; Eyring, E. M.; Petrucci, S., unpublished data.
- (11) Fuoss, R. M. *J. Am. Chem. Soc.* 1958, 80, 5059.
- (12) Data for affinity in methanol for 12C4 + Na^+ give $K_2 = 29.3$ or $K_2 = 56.6$ (depending on the source) and for 15C5 + Na^+ give $K_2 = 1860$ (averaging all the reported data). From *Cation Binding by Macrocycles*, Inoue, Y., Gokel, G. W., Eds.; Marcel Dekker: New York, 1990; Chapter 1, pp 11-13.
- (13) Takeda, Y. In *Cation Binding by Macrocycles*, Inoue, Y., Gokel, G. W., Eds.; Marcel Dekker: New York, 1990; Chapter 3, pp 146, 174.
- (14) Tamm, K. In *Dispersion and Absorption of Sound by Molecular Processes*; Sette, D., Ed.; Academic Press: New York, 1963; p 192.
- (15) For a discussion of this function see: Inoue, N.; Xu, M.; Petrucci, S. *J. Phys. Chem.* 1987, 91, 4628. See also ref 16.
- (16) Maaser, H.; Xu, M.; Hemmes, P.; Petrucci, S. *J. Phys. Chem.* 1987, 91, 3047.
- (17) Bright, D.; Truter, R. M. *Nature* 1970, 225, 176; *J. Chem. Soc.* 1970, 1544.

Excited-State Interactions in Ligand-Bridged Chromophore-Quencher Complexes Containing Rhodium(III) and Ruthenium(II) Polypyridyl Units

K. Kalyanasundaram,* M. Grätzel, and Md. K. Nazeeruddin

Institut de Chimie Physique, Ecole Polytechnique Fédérale, CH-1015 Lausanne, Switzerland

(Received: January 14, 1992)

This work consists of two parts: (i) photophysical studies on the mononuclear Rh(III)-polypyridyl complexes ($[\text{Rh}(\text{dpp})_2\text{Cl}_2]^+$, $[\text{Rh}(\text{bpy})_2(\text{dpp})]^{3+}$, and $[\text{Rh}(\text{dpp})_2(\text{bpy})]^{3+}$) and (ii) an examination of the intramolecular excited-state interactions in the ligand-bridged complex, $[(\text{bpy})_2\text{Ru}^{\text{II}}-\text{dpp}-\text{Rh}^{\text{III}}(\text{bpy})_2]^{5+}$ using luminescence and transient absorption spectral studies. Over the temperature range 77-293 K, the lowest excited state of $[\text{Rh}(\text{dpp})_2\text{Cl}_2]^+$ is metal-centered (MC or d-d). At 77 K, mixed ligand complexes $[\text{Rh}(\text{bpy})_2(\text{dpp})]^{3+}$ and $[\text{Rh}(\text{dpp})_2(\text{bpy})]^{3+}$ show strong emission from ligand-centered (LC or $\pi-\pi^*$) and a very weak one from metal-centered excited states. Lifetime studies indicate the two low-lying excited states to be nonequilibrated in rigid alcoholic glasses. Only very weak (π,π^*) emission is observed in fluid solutions (293 K). Distinct transient absorption following short laser pulse excitation allows establishment of spectra and lifetimes of these excited states in fluid solutions at ambient temperature. Visible light excitation of the mixed metal Rh-dpp-Ru complex leads to formation of the luminescent charge-transfer (CT) excited state of Ru(II)-polypyridyl based chromophore. The very short lifetime of this excited state species in fluid solutions as compared to model compounds can be caused by enhanced nonradiative decay (mechanism I) or by intramolecular electron-transfer or energy-transfer quenching (mechanisms II and III, respectively) involving an adjacent Rh(III)-polypyridyl unit. Analysis of the quenching pathways using the electrochemical and photophysical data on the mixed metal and relevant mononuclear complexes leads to the conclusion that the quenching is primarily by electron transfer (mechanism II).

Introduction

There has been enormous progress in the past 2 decades in our understanding of the photophysics of transition metal polypyridyl complexes.^{1,2} This has allowed extension of these studies to larger "supramolecular systems" tailored to have required properties.³ Ligand-bridged polynuclear complexes constitute one such su-

pramolecular assembly, and these are currently receiving intense scrutiny. Progress in this area can lead to a better understanding of the chemistry of mixed valence species, communication through bridging ligands, antenna systems, and electron-transfer processes. We⁴ and others^{5,6} have been investigating the photophysical and redox properties of polynuclear polypyridyl complexes of the type